

Entangled X-Ray Photon Pair Generation by Free-Electron Lasers

Linfeng Zhang^{1,*}, Zunqi Li^{1,*}, Dongyu Liu^{1,2}, Chengyin Wu^{1,3,4}, Haitan Xu^{5,6,7,†} and Zheng Li^{1,3,4,‡}

¹State Key Laboratory for Mesoscopic Physics and Frontiers Science Center for Nano-optoelectronics, School of Physics, Peking University, Beijing 100871, China

²Physics Department, Stanford University, California 94305, USA

³Collaborative Innovation Center of Extreme Optics, Shanxi University, Taiyuan, Shanxi 030006, China

⁴Peking University Yangtze Delta Institute of Optoelectronics, Nantong, Jiangsu 226010, China

⁵School of Materials Science and Intelligent Engineering, Nanjing University, Suzhou, Jiangsu 215163, China

⁶Shishan Laboratory, Nanjing University, Suzhou, Jiangsu 215163, China

⁷School of Physical Sciences, University of Science and Technology of China, Hefei, Anhui 230026, China

 (Received 7 March 2023; revised 6 June 2023; accepted 14 July 2023; published 14 August 2023)

We investigate entangled x-ray photon pair emissions in a free-electron laser (FEL) and establish a quantum electrodynamical theory for coherently amplified entangled photon pair emission from microbunched electron pulses in the undulator. We provide a scheme to generate highly entangled x-ray photon pairs and numerically demonstrate the properties of entangled emission, which is of great importance in x-ray quantum optics. Our work shows a unique advantage of FELs in entangled x-ray photon pair generation.

DOI: 10.1103/PhysRevLett.131.073601

The prediction of Einstein *et al.* [1] on incompleteness of quantum mechanics was overturned by experimental tests on Bell's inequality [2] that confirmed the existence of quantum entanglement. In x-ray optics, entangled photon pairs can be generated by the Unruh effect [3], nuclear forward scattering [4], or x-ray parametric down-conversion [5]. Meanwhile, free-electron lasers (FELs) have successfully lased at x-ray frequencies recently [6–12].

Being an ultrabright and ultrashort x-ray laser source, FELs have shed light on various research areas, including single-particle imaging [13–15], ultrafast x-ray spectroscopy [16–18], and high-energy density physics [19–21]. The FEL emission was mostly seen as a classical phenomenon with minor quantum corrections [22]. However, a critical quantum effect, i.e., the quantum entanglement, has never been investigated for the x-ray emission from the FEL.

In this Letter, we study the entangled x-ray photon pairs generated by the microbunched electrons in the undulator, rather than the electrons in the laser field [3], the nuclei [4], or the electrons in nonlinear crystals [5]. We start by presenting the quantum electrodynamics (QED) treatment of photon pair emission from a single electron in the undulator and calculate the cross section and the entanglement degree. Then we apply the Feynman rules to microbunched electrons, which takes into account the many-body effect, to analyze the coherent amplification and establish the condition for coherence. We further numerically investigate the enhancement of entangled photon pair emission by microbunched electrons.

We present in Fig. 1 the quantum mechanism of entangled x-ray photon pair emission. Figure 1(a) shows

a typical self-amplification of spontaneous emission (SASE) FEL process in the lab frame. A relativistic electron pulse travels through an undulator, interacts with the

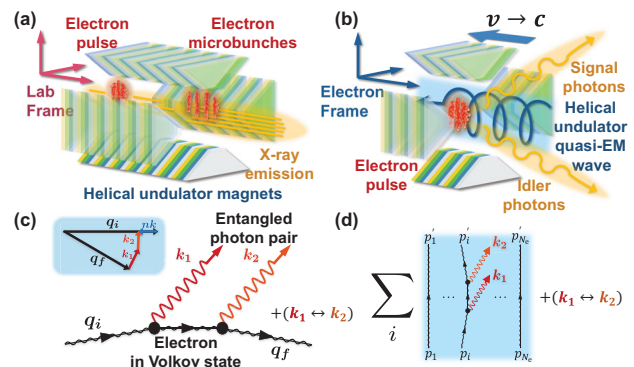


FIG. 1. Mechanism of coherent entangled x-ray photon pair emission in a SASE FEL. (a) Schematic in the lab frame, where a relativistic electron pulse (red) passes through an undulator, causing photon emission (yellow) while being microbunched. The fundamental frequency of the emission can reach the x-ray region, with single-photon energy of hundreds of eVs. The schematic of the helical undulator is drawn according to the configuration of the Delta undulator at the LCLS [23]. (b) Schematic in the electron frame, where the electron pulse is initially at rest. The strong quasi-EM wave (blue) of the relativistic undulator is scattered from the electrons. The resulting emission contains multiple components, including single-photon emission, double-photon emission, etc. (c) The Feynman diagrams corresponding to double-photon emission in the electron frame. The black lines refer to the Volkov states of electrons. Inset: a typical constraint of four-momenta of the particles. n is the net number of Floquet photons absorbed. (d) Coherent summation of Feynman diagrams with $n = 1$, including permutations of k_1 and k_2 .

electromagnetic (EM) field of the undulator, resulting in electron microbunching and amplified emission.

To facilitate the study of entangled photon emission from the FEL, we use the electron frame (EF), where the incident electron pulse has a zero initial average velocity. We adopt the frame transformation formalism from the Weizsäcker-Williams method [24] and use the natural units $\hbar = c = \epsilon_0 = 1$. For a helical undulator, $A_{\text{Lab}}^\mu = a(0, \cos(k_u x_{\text{Lab}}^3), \sin(k_u x_{\text{Lab}}^3), 0)$, where $a = B_0/k_u$, B_0 is the amplitude of the undulator field, and $k_u = 2\pi/\lambda_u$ is the spatial frequency of the undulator with a period of λ_u in the lab frame [25]. The undulator field is transformed to a quasi-EM wave in the EF by the Lorentz boost as $A_{\text{EF}}^\mu = a(0, \cos[k_u(\gamma\beta x_{\text{EF}}^0 + \gamma x_{\text{EF}}^3)], \sin[k_u(\gamma\beta x_{\text{EF}}^0 + \gamma x_{\text{EF}}^3)], 0) = a(0, \cos(k \cdot x_{\text{EF}}), \sin(k \cdot x_{\text{EF}}), 0)$, where β and γ are the average velocity and Lorentz factor of the electron pulse. $k = \gamma k_u(\beta, 0, 0, -1)$ is the wave vector of the undulator quasi-EM wave in the EF, which is close to the photon mass shell for $\beta \rightarrow 1$. The helical undulator is practically available, such as the Delta undulator at the Linac Coherent Light Source (LCLS) [23].

The SASE emission can be approximated as the scattering of the quasi-EM wave from the electron pulse in the EF. The emission takes part in the microbunching of the electron pulse and is significantly enhanced at the fundamental frequency and its harmonics. In the lab frame, the fundamental frequency $\omega_{\text{fd}} = 2\gamma^2(2\pi/\lambda_u)/(1 + K^2)$ for the helical undulator, where $K = eB_0/mk_u = ea/m$ is the undulator parameter [6,22,26].

For strong undulator quasi-EM wave, nonlinear scattering can be observed in the emission. We focus on the double-scattering processes, as shown in Fig. 1(b). In this Letter, we use the FEL parameters of the LCLS [6], as shown in Table I.

For a representative electron initially at rest in the EF, it satisfies the Dirac equation $(\not{p} - e\not{A} - m)\Psi = 0$, where $\not{p} = \gamma^\mu p_\mu$, γ^μ are the Dirac matrices, A is the EM four-potential, e is the electron charge, and m is the rest electron mass.

In the undulator quasi-EM wave, the electron is in a Volkov state $\Psi_p^V(x) = \{1 - [e\not{A}\not{k}/(2k \cdot p)]\}u_p \times \exp\{-i[p \cdot x + \int_0^\phi (\{[e p \cdot A(\phi')]/(k \cdot p)\} - [e^2 A^2(\phi')/(2k \cdot p)])d\phi'\}$, where $\phi = k \cdot x = k^\mu x_\mu = k^0 x^0 - \mathbf{k} \cdot \mathbf{x}$, u_p is the free-electron spinor, and $A \simeq A_{\text{EF}}$ (see Ref. [27], Sec. I). For an electron

of initial four-momentum p , the corresponding Volkov state has a time-varying four-momentum whose average is the quasi-momentum $q^\mu = p^\mu + [e^2 a^2/(2k \cdot p)]k^\mu$, satisfying $|q|^2 = m^2 + e^2 a^2 = m_*^2$.

In the Floquet picture, the Volkov state corresponds to the superposition state of the electron dressed by \tilde{n} Floquet photons, i.e., $\Psi_p^V(x) = \sum_{\tilde{n}=-\infty}^{+\infty} F_{\tilde{n}} \exp\{-i(q \cdot x + \tilde{n}k \cdot x)\}u(p)$ (the expression of $F_{\tilde{n}}$ can be found in the Supplemental Material, see Ref. [27], Sec. II.A). The electron in the Volkov state can spontaneously decay into another Volkov state with a different quasimomentum and thus radiate photons [33,34], the amplitude of which can be evaluated by the Feynman diagrams (see Ref. [27], Sec. II). Especially, the entangled photon pair emission satisfies the four-momentum conservation $q_f + k_1 + k_2 - q_i - nk = 0$ [see Fig. 1(c)]. k_1 and k_2 are the momentum of entangled photons, and n corresponds to the number of Floquet photons absorbed. As the energies of photons (k^0, k_1^0, k_2^0) are much less than the electron mass (m) and the quasimomenta (q_i, q_f) in the EF when n is reasonably small, the four-momentum conservation leads to $k_1^0 + k_2^0 \simeq nk^0$. We focus on the representative case of $n = 1$, which corresponds to photon pairs with total frequency of ω_{fd} in the lab frame and can be distinguished from other cases with different n by detecting the emitted photon pair energies (see Ref. [27], Sec. III).

With the above treatment, we obtain the scattering matrix element S_{fi} for the process from an initial Volkov state i to any final Volkov state f emitting a pair of photons in plane wave states with arbitrary polarization or helicity. The differential double-photon emission rate is given by

$$\frac{d\dot{W}}{dk_1^0 d\Omega_{k_1} d\Omega_{k_2}} = \frac{e^4 m^2}{(2\pi)^5 2q_i^0} \times \sum_{n=1}^{+\infty} \frac{k_1^0 (k_2^0)^2 \Theta(q_i^0 + nk^0 - k_1^0 - k_2^0) M}{2|(q_i + nk - k_1) \cdot k_2|} \Big|_{\text{DE}(n)}, \quad (1)$$

where Ω_{k_1} and Ω_{k_2} are the solid angles of the emitted photon pair, the notation $|_{\text{DE}(n)}$ represents the constraint of $(q_i + nk - k_1) \cdot k_2 = q_i \cdot nk - q_i \cdot k_1 - nk \cdot k_1$, and the helicity-relevant part M is explained in the Supplemental Material (see Ref. [27], Sec. II).

In order to quantify the entanglement degree of the emitted x-ray photon pairs, we calculate the density matrix ρ_f in the helicity basis from the scattering matrix elements S_{fi} as $\rho_f = \frac{1}{2} \sum_{r_i, r_f=1}^2 N(S_{fi, j_1} S_{fi, j_2}^*)_{4 \times 4}$, where S_{fi, j_1} and S_{fi, j_2} represent the scattering matrix elements with the emitted photon pair at helicity eigenstates j_1 and j_2 , and $j_1, j_2 = 1, 2, 3, 4$ correspond to the helicity eigenstates $|++\rangle, |+-\rangle, |-+\rangle$, and $|--\rangle$, where \pm corresponds to the right- and left-handed helicity [35]. N is chosen to keep

TABLE I. FEL parameters used in this Letter, based on LCLS [6].

Electron energy	5 GeV	Undulator period number	1392
Charge per pulse	180 pC	Pierce parameter	2×10^{-3}
Peak current	3.4 kA	Fundamental wavelength	2.30 nm
Repetition rate	120 Hz	Saturation peak power	10 GW
Undulator field	1.32 T	Emission pulse FWHM	230 fs
Undulator period	30 mm		

$\text{Tr}[\rho_f] = 1$. r_i and r_f represent the spin of the electron at initial and final states, respectively, which have been traced out. The scattering matrix elements can be calculated for any choice of k_1, k_2 satisfying the constraint $(k_1 + k_2 - q_i - nk)^2 - m_*^2 = 0$.

To characterize the quantum entanglement of the emitted photon pair, we use the so-called concurrence as a measure of the entanglement [36]. The concurrence can be calculated from the density matrix as

$$C(\rho_f) = \max(0, \sqrt{\zeta_1} - \sqrt{\zeta_2} - \sqrt{\zeta_3} - \sqrt{\zeta_4}), \quad (2)$$

where $\zeta_{1,2,3,4}$ are the four eigenvalues of the matrix $Q = \rho_f(\sigma^2 \otimes \sigma^2)\rho_f^*(\sigma^2 \otimes \sigma^2)$ in descending order, and σ^2 is one of the Pauli matrices. $C \in [0, 1]$, with $C = 0$ corresponding to a unentangled state and $C = 1$ corresponding to a fully entangled state. As the helicity of photons are Lorentz invariant, the density matrix and the concurrence are also Lorentz invariant.

We have represented the density matrix and the concurrence of the 2-qubit states of the emitted photon pairs with the basis of the helicity eigenstates $|++\rangle, |+-\rangle, |-+\rangle, |--\rangle$. The choice of basis is not unique, and we can alternatively choose other basis states, such as linear polarization eigenstates [35], which result in a unitary transformation of the density matrix, and the concurrence remains invariant (see Ref. [27], Sec. VII). In addition, we can choose other entanglement monotones instead of the concurrence to quantify the entanglement degree, such as entanglement of formation and negativity. A comparison showing qualitative agreement between these entanglement measures and the concurrence is given in the Supplemental Material (see Ref. [27], Sec. IX).

After the discussion about the entangled photon pair emission from a single electron in the undulator, we proceed to the entangled photon pair emission from microbunched electrons in the FEL, which is a collective many-electron phenomenon. In the high-gain regime of the FEL, a coherent enhancement due to the electron microbunching plays a vital role. For a sufficiently bright electron beam and a sufficiently long undulator, the combination of the undulator field and the radiation field will induce a ponderomotive potential modulating the energy of the electron beam [26]. This energy modulation eventually forces the electrons to form periodic microbunches along the undulator axis with a modulation wavelength $\lambda_1 = 2\pi/\omega_{\text{fd}}$ equal to the fundamental wavelength.

The conventional analysis of the coherence property due to the microbunching relies on the paraxial wave equation [26], which cannot explain the quantum phenomenon of entangled photon pair emission. To overcome this problem, we develop a quantum collective double-emission (QCDE) theory for the rigorous analysis of entangled emission from microbunched electrons in the FEL undulator (see Ref. [27], Sec. IV). This theory provides a QED description

of the microbunched state of electrons and deals with the interference of the Feynman diagrams corresponding to double emissions from different electrons. The collective double-emission rate in the QCDE theory is

$$\left(\frac{d\dot{W}}{dk_1^0 d\Omega_{k_1} d\Omega_{k_2}} \right)_C = \frac{d\dot{W}}{dk_1^0 d\Omega_{k_1} d\Omega_{k_2}} F_{\text{MB}}(Z'_1, Z'_2, k_1^0), \quad (3)$$

where $F_{\text{MB}}(Z'_1, Z'_2, k_1^0)$ is the enhancement factor on the emission rate introduced by microbunching. $(d\dot{W}/dk_1^0 d\Omega_{k_1} d\Omega_{k_2})_C$ represents the collective differential emission rate for a microbunched electron pulse. In addition to the rigorous QCDE theory presented in the Supplemental Material [27], here we elaborate on the physical picture leading to the coherent enhancement factor $F_{\text{MB}}(Z'_1, Z'_2, k_1^0)$ via an analogy with the quasi-phase-matching in nonlinear optics (see Ref. [27], Sec. IV).

In the electron frame, we can view the quasi-EM wave generated by the relativistic undulator as the pump and the emitted photon pair as the signal and idler. The electron microbunches can be regarded as a nonlinear medium with periodic structure. Therefore, the phase difference between photons emitted by adjacent microbunches should be equal to $\Delta\phi = \Delta l \cdot \Delta k$, where $\Delta l = |\Delta l| \hat{e}^3 = (\lambda_u/\gamma)[(1 + K^2)/(2 + K^2)] \hat{e}^3$ is the average relative displacement between adjacent microbunches, with \hat{e}^3 being the unit vector along the undulator, and $\Delta k = k_1 + k_2 - nk$ is the momentum transfer between the pump photon and the emitted photon pair.

If the momenta of the signal and idler photons are both along the x^3 axis, the total momentum of the photon pair is $k_1 + k_2 = -nk/(1 + K^2)$. Therefore, the phase difference is exactly $\Delta\phi = 2\pi n$, resulting in a fully constructive interference between emissions from different electron microbunches and hence an N_e^2 enhancement of the collective emission rate. In a practical FEL system, the situation deviates from the ideal one, and only adjacent microbunches within the coherence length contribute to the constructive interference, the number of which is estimated to be about $N_c = 22$ for the parameters shown in Table I.

Meanwhile, if the directions of the emitted photon pair are away from the x^3 axis, the phase difference will deviate from $2\pi n$ with a nontrivial angular dependence $\Delta\phi(Z'_1, Z'_2, k_1^0) = 2\pi((1 + K^2)\{1 + \cos(Z'_2) - [\cos(Z'_2) - \cos(Z'_1)]k_1^0/k^0\}/\{2 + K^2[1 + \cos(Z'_2)]\})$ (see Ref. [27], Sec. IV), where Z'_1, Z'_2 are the zenith angles of the two emitted photons relative to the x^3 axis in the electron frame. The enhancement parameter on the scattering amplitude by electron microbunches within one coherent length is given by $H(Z'_1, Z'_2, k_1^0) = \sum_{j=1}^{N_c} N_j e^{i[j\Delta\phi(Z'_1, Z'_2, k_1^0)]}$, where N_j is the number of electrons within the j th electron microbunch. The collective emission rate of such coherent microbunches is the product of the emission rate from a single electron and the enhancement parameter $|H(Z'_1, Z'_2, k_1^0)|^2$. For the

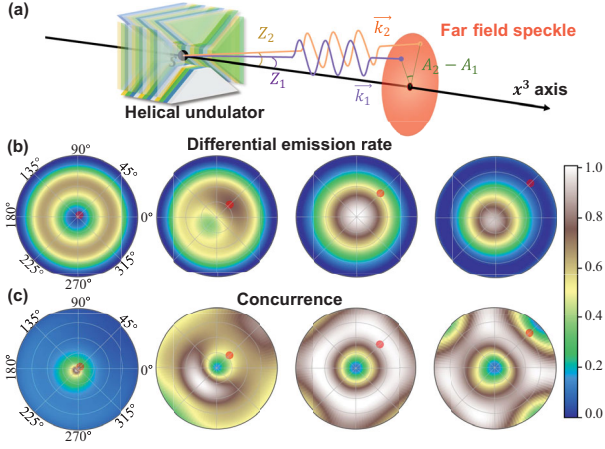


FIG. 2. Numerical simulation of entangled x-ray photon pair emission with microbunch enhancement. (a) Illustration of the angles in (b) and (c). $Z_{1,2}$ refer to the zenith angle between the three-momentum $\mathbf{k}_1, \mathbf{k}_2$ of the emitted photons and the x^3 axis. $A_{1,2}$ refer to the azimuth angles of the emitted photons at the transverse far field plane. In the helical undulator, only $A_2 - A_1$ matters. The angles are defined with respect to the point S at the center of the undulator for far field measurement. (b) Normalized double-angular distribution of the differential emission rate $d\dot{W}/dk_1^0 d\Omega_{k_1} d\Omega_{k_2}$ in the lab frame. (c) Double-angular distribution of the concurrence \mathcal{C} . In both (b) and (c) the polar angle refers to $A_2 \in [0, 2\pi]$, and the radii refer to $\gamma \tan(Z_2) \in [0, 1]$ for photon 2. The red points represent the directions of photon 1. Here we choose $\omega_1 \simeq \omega_{\text{fd}}/3$.

entire electron pulse, the coherent enhancement factor in Eq. (3) is given by

$$F_{\text{MB}} = |H(Z'_1, Z'_2, k_1^0)|^2 N_i, \quad (4)$$

where $N_i \simeq N_e / (\sum_{j=1}^{N_c} N_j)$ represents the approximate number of coherent sections.

In addition, using the Lorentz transformation $\gamma \tan(Z'_l) = \sin(Z'_l) / [\beta + \cos(Z'_l)]$, we can determine the zenith angles Z_1 and Z_2 in the lab frame for observation of the entangled photon pair emission. As the density matrix of the emitted photon pairs from microbunched electrons has an identical form as that from the single-electron emission, the entanglement degree is retained under microbunching enhancement.

We then calculate the total emission rate \dot{W}_{fi} . We set practical ranges of photon energies and angular directions for both photon detectors and focus on the case of $n = 1$. The relevant angles are illustrated in Fig. 2(a). For the helical undulator, the dependence on the azimuthal angles A_1, A_2 of the emitted photon pair can be simplified to $A_2 - A_1$. Choosing $\omega_1 \simeq \omega_{\text{fd}}/3$ and $\omega_2 \simeq 2\omega_{\text{fd}}/3$ in the lab frame, the double-angular distribution of the differential emission rate $d\dot{W}/dk_1^0 d\Omega_{k_1} d\Omega_{k_2}$ is shown in Fig. 2(b). Here, we show the distribution with respect to Z_2, A_2 in polar figures for certain directions of photon 1 labeled by

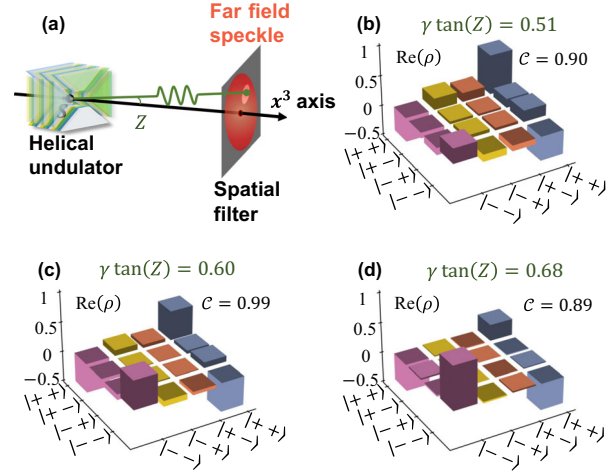


FIG. 3. Density matrices of the emitted photon pairs. (a) Geometry of the inserted circular aperture, where Z describes the angular position of the circular hole relative to the point S . (b)–(d) Real parts of the density matrices of the resulting entangled states for the aperture shown in (a) with $\gamma \tan(Z) = 0.51, 0.60, 0.68$, which leads to $\mathcal{C} = 0.90, 0.99, 0.89$, respectively. The size of the circular aperture is chosen to be $\sim 1/240$ of the far field speckle. The imaginary parts of the density matrices are zero due to the specific choice of the helicity basis and the identical emitting directions of the entangled photons (see Ref. [27], Sec. VIII).

the red points. The polar angles refer to $A_2 \in [0, 2\pi]$, and the radii refer to $\gamma \tan(Z_2) \in [0, 1]$ for photon 2. The entangled emission probability has an explicit relation with the key parameters of the FEL undulator, γ, λ_u , and B_0 , which is given in the Appendix.

To demonstrate the quantum entanglement, we show the concurrence \mathcal{C} of the emitted photon pairs with respect to Z_2, A_2 for certain directions of photon 1 labeled by the red points in Fig. 2(c), corresponding to the plots in Fig. 2(b). Especially, \mathcal{C} can reach its upper limit of 1 for certain angles, meaning that fully entangled two-photon states may be generated. Concurrence close to 1 can be approached at multiple angles. However, for most regions in the double-angular parameter space, the concurrence is relatively low. Thus, without selection or purification, the overall entanglement of the emitted photon pairs would vanish.

To obtain higher concurrence, a circular aperture can be inserted into the system at far field as shown in Fig. 3(a), and only photon pairs that are emitted in the direction $Z_2 \simeq Z_1 \simeq Z$ can pass through the aperture. In light of the numerical calculation for the angular distribution of concurrence shown in Fig. 2(b), the circular aperture can be chosen to maximize the concurrence of the photon pairs that pass it. As demonstrated in Figs. 3(b)–3(d), concurrence close to 1 can be achieved at multiple angles such as $\gamma \tan(Z) = 0.51, 0.60, 0.68$ with a sufficiently small aperture, whose size is chosen to be $\sim 1/240$ of the far field speckle.

The helical undulator simplifies the dependence of the double-emission process on the emitting azimuth angles A_1, A_2 to $A_2 - A_1$ and reduces the parameter space, making it more convenient to investigate and generate the highly entangled photon pairs. A detailed calculation for the case of linearly polarized undulator is given in the Supplemental Material (see Ref. [27], Sec. VI).

We can now estimate the emission rate of the entangled photon pairs in certain energy ranges that pass through the aperture in the lab frame. We consider the double emission after saturation of the SASE process, which can be achieved by using two cascaded undulators of the same parameters and use a chicane and a monochromator in between. The energy ranges of the emitted photons are chosen to be $[\omega_{fd}/3-10 \text{ eV}, \omega_{fd}/3]$ and $[2\omega_{fd}/3-10 \text{ eV}, 2\omega_{fd}/3]$, which are [170, 180] and [350, 360] eV, and the fundamental frequency is 540 eV. The angular position of the circular hole is chosen to be $\gamma \tan(Z) = 0.60$. After the aperture, the solid angles of the emitted photons are much smaller than that of the detectors, which ensures the detection of the entangled photons.

For single electrons, the emission rate of the entangled photon pairs is $R_{SE} = 2.8 \times 10^{-24}$ per electron. For microbunched electron pulses in the FEL with $N_e = 1.12 \times 10^9$ as in Table I, we estimate the number of electrons in each microbunch to be a typical value of 10^6 . With Eq. (3), we obtain a rate of $R_{FEL} = 2.6 \times 10^{-8}$ per electron pulse. Our analysis can also be applied to synchrotrons. For electron pulses in a synchrotron, with the number of electrons per pulse $N_e = 1.12 \times 10^9$, the total emission rate is $R_{Sync} = N_e R_{SE} = 3.1 \times 10^{-15}$ per electron pulse. The total emission rate also depends on the actual repetition rate of the electron pulses, which is improving over time.

As we focus on the double emissions whose frequencies are far away from the fundamental frequency, the background noise mainly contributed by the single emission is much smaller than that around the fundamental frequency. In addition, the signal-to-noise ratio can be further improved by tapering the undulator.

In conclusion, we have theoretically demonstrated the entangled photon pair generation with FEL. In the electron frame, the double-photon emission can be understood as the scattering between the electrons and the quasi-EM wave of the undulator field, which can be enhanced by the electron microbunching in FEL. We demonstrate that the FEL can generate highly entangled photon pairs with enhanced emission rate, which is impossible from a classical perspective. The FEL can thus be utilized as an entangled photon pair source for x-ray quantum optics, especially for applications in the soft x-ray regime where it is challenging to use nonlinear effects like spontaneous parametric down-conversion due to the strong absorption in nonlinear crystals.

The authors thank Zhirong Huang and Zhaoheng Guo for helpful discussions. This work was supported by the

National Natural Science Foundation of China (No. 12174009, No. 11974031, No. 12174011, No. 12234002, No. 92250303), Innovation Program for Quantum Science and Technology (No. 2021ZD0301702), Beijing Natural Science Foundation (No. Z220008), and funding from the State Key Laboratory for Mesoscopic Physics.

Appendix: Dependence of double-emission probability on key parameters of FEL undulator.—In order to explicitly show the dependence of the entangled emission probability on the key FEL parameters, we can reduce the formula of the differential entangled double-emission probability for a single electron in the lab frame based on Eq. (1). Focusing on $n = 1$, the entangled emission probability U_{pair} is given by

$$U_{\text{pair}} \simeq F_L F_S \frac{d\dot{W}}{dk_1^0 d\Omega_{k_1} d\Omega_{k_2}} \Big|_{\text{EF}, k_1, k_2}, \quad (\text{A1})$$

where $(d\dot{W}/dk_1^0 d\Omega_{k_1} d\Omega_{k_2})|_{\text{EF}, k_1, k_2}$ is the value of differential emission rate in Eq. (1) with the two-photon four-momenta in EF chosen as k_1, k_2 , and F_L, F_S are the prefactors related to the Lorentz transformation and solid angle, respectively.

U_{pair} can be expressed with key FEL parameters γ, λ_u , and B_0 , which represent the Lorentz factor of electrons, undulator period length, and magnetic field amplitude of the undulator, in the form of

$$U_{\text{pair}} \propto \frac{Q(B_0 \lambda_u)}{\lambda_u^2 [1 + (c_K B_0 \lambda_u)^2]^2 [1 + (c_K B_0 \lambda_u)^2 / 2]} \times \frac{1}{[1 + (c_K B_0 \lambda_u)^2 (1 + \cos Z'_2) / 2]}, \quad (\text{A2})$$

where

$$Q(B_0 \lambda_u) = \sum_{t_1, t_2, t_3, t_4=0}^2 P_{t_1, t_2, t_3, t_4}(B_0 \lambda_u) \times J_{t_1} \left(\sin Z'_1 \frac{(c_K B_0 \lambda_u)}{1 + (c_K B_0 \lambda_u)^2} \right) \times J_{t_2} \left(\sin Z'_1 \frac{(c_K B_0 \lambda_u)}{1 + (c_K B_0 \lambda_u)^2} \right) \times J_{t_3} \left(\sin Z'_2 \frac{(c_K B_0 \lambda_u)}{1 + (c_K B_0 \lambda_u)^2} \right) \times J_{t_4} \left(\sin Z'_2 \frac{(c_K B_0 \lambda_u)}{1 + (c_K B_0 \lambda_u)^2} \right),$$

and $c_K = e/2\pi m$. $P_{t_1, t_2, t_3, t_4}(B_0 \lambda_u)$ are polynomials of $B_0 \lambda_u$ with the highest order between 4 and 8, and $J_t(x)$ refers to the Bessel function of the first kind with order t . The detailed derivation of Eq. (A2) is presented in the

Supplemental Material (see Ref. [27], Sec. V). At the vicinity of a specific choice of k_1, k_2 , we can obtain an approximated power function for $Q(B_0\lambda_u)$. For example, consider k_1, k_2 that satisfy $\omega_1 = \omega_{fd}/3$ and $\gamma \tan Z_{1,2} \simeq 0.51, 0.60, 0.68$ in the lab frame, with the corresponding $\omega_2 \simeq 2\omega_{fd}/3$ given by the conservation of four-quasimomentum. These three cases correspond to the three circumstances shown in Fig. 3 of the main text. We obtain by fitting that $Q(B_0\lambda_u) \propto (B_0\lambda_u)^\alpha$, while $\alpha \simeq 1.90, 2.00, 2.10$ for $\gamma \tan Z_{1,2} \simeq 0.51, 0.60, 0.68$, respectively. The details are shown in the Supplemental Material (see Ref. [27], Sec. V).

*L. Z. and Z. L. contributed equally to this work.

†haitanxu@nju.edu.cn

‡zheng.li@pku.edu.cn

- [1] A. Einstein, B. Podolsky, and N. Rosen, Can quantum-mechanical description of physical reality be considered complete?, *Phys. Rev.* **47**, 777 (1935).
- [2] J. S. Bell, On the problem of hidden variables in quantum mechanics, *Rev. Mod. Phys.* **38**, 447 (1966).
- [3] R. Schützhold, G. Schaller, and D. Habs, Tabletop Creation of Entangled Multi-keV Photon Pairs and the Unruh Effect, *Phys. Rev. Lett.* **100**, 091301 (2008).
- [4] A. Pálffy, C. H. Keitel, and J. Evers, Single-Photon Entanglement in the keV Regime via Coherent Control of Nuclear Forward Scattering, *Phys. Rev. Lett.* **103**, 017401 (2009).
- [5] S. Schwartz, R. N. Coffee, J. M. Feldkamp, Y. Feng, J. B. Hastings, G. Y. Yin, and S. E. Harris, X-Ray Parametric Down-Conversion in the Langevin Regime, *Phys. Rev. Lett.* **109**, 013602 (2012).
- [6] P. Emma, R. Akre, J. Arthur, R. Bionta, C. Bostedt, J. Bozek, A. Brachmann, P. Bucksbaum, R. Coffee, F. J. Decker *et al.*, First lasing and operation of an ångström-wavelength free-electron laser, *Nat. Photonics* **4**, 641 (2010).
- [7] T. Ishikawa, H. Aoyagi, T. Asaka, Y. Asano, N. Azumi, T. Bizen, H. Ego, K. Fukami, T. Fukui, Y. Furukawa *et al.*, A compact x-ray free-electron laser emitting in the sub-ångström region, *Nat. Photonics* **6**, 540 (2012).
- [8] E. Allaria, D. Castronovo, P. Cinquegrana, P. Craievich, M. Dal Forno, M. B. Danailov, G. D’Auria, A. Demidovich, G. De Ninno, S. Di Mitri *et al.*, Two-stage seeded soft-x-ray free-electron laser, *Nat. Photonics* **7**, 913 (2013).
- [9] W. Wang, K. Feng, L. Ke, C. Yu, Y. Xu, R. Qi, Y. Chen, Z. Qin, Z. Zhang, M. Fang *et al.*, Free-electron lasing at 27 nanometres based on a laser wakefield accelerator, *Nature (London)* **595**, 516 (2021).
- [10] R. Pompili, D. Alesini, M. P. Anania, S. Arjmand, M. Behtouei, M. Bellaveglia, A. Biagioni, B. Buonomo, F. Cardelli, M. Carpanese *et al.*, Free-electron lasing with compact beam-driven plasma wakefield accelerator, *Nature (London)* **605**, 659 (2022).
- [11] J. Duris, S. Li, T. Driver, E. G. Champenois, J. P. MacArthur, A. A. Lutman, Z. Zhang, P. Rosenberger, J. W. Aldrich, R. Coffee *et al.*, Tunable isolated attosecond x-ray pulses with gigawatt peak power from a free-electron laser, *Nat. Photonics* **14**, 30 (2020).
- [12] J. P. Duris, J. P. MacArthur, J. M. Glowia, S. Li, S. Vetter, A. Miahnahri, R. Coffee, P. Hering, A. Fry, M. E. Welch *et al.*, Controllable X-Ray Pulse Trains from Enhanced Self-Amplified Spontaneous Emission, *Phys. Rev. Lett.* **126**, 104802 (2021).
- [13] M. M. Seibert, T. Ekeberg, F. R. N. C. Maia, M. Svenda, J. Andreasson, O. Jönsson, D. Odić, B. Iwan, A. Rocker, D. Westphal *et al.*, Single mimivirus particles intercepted and imaged with an x-ray laser, *Nature (London)* **470**, 78 (2011).
- [14] N. D. Loh, C. Y. Hampton, A. V. Martin, D. Starodub, R. G. Sierra, A. Barty, A. Aquila, J. Schulz, L. Lomb, J. Steinbrener *et al.*, Fractal morphology, imaging and mass spectrometry of single aerosol particles in flight, *Nature (London)* **486**, 513 (2012).
- [15] L. F. Gomez, K. R. Ferguson, J. P. Cryan, C. Bacellar, R. M. P. Tanyag, C. Jones, S. Schorb, D. Anielski, A. Belkacem, C. Bernardo *et al.*, Shapes and vorticities of superfluid helium nanodroplets, *Science* **345**, 906 (2014).
- [16] J. Kern, R. Alonso-Mori, R. Tran, J. Hattné, R. J. Gildea, N. Echols, C. Glöckner, J. Hellmich, H. Laksmo, R. G. Sierra *et al.*, Simultaneous femtosecond x-ray spectroscopy and diffraction of photosystem II at room temperature, *Science* **340**, 491 (2013).
- [17] B. Erk, R. Boll, S. Trippel, D. Anielski, L. Foucar, B. Rudek, S. W. Epp, R. Coffee, S. Carron, S. Schorb *et al.*, Imaging charge transfer in iodomethane upon x-ray photo-absorption, *Science* **345**, 288 (2014).
- [18] B. Rudek, S. Son, L. Foucar, S. W. Epp, B. Erk, R. Hartmann, M. Adolph, R. Andritschke, A. Aquila, N. Berrah *et al.*, Ultra-efficient ionization of heavy atoms by intense x-ray free-electron laser pulses, *Nat. Photonics* **6**, 858 (2012).
- [19] S. M. Vinko, O. Ciricosta, B. I. Cho, K. Engelhorn, H.-K. Chung, C. R. D. Brown, T. Burian, J. Chalupský, R. W. Falcone, C. Graves *et al.*, Creation and diagnosis of a solid-density plasma with an x-ray free-electron laser, *Nature (London)* **482**, 59 (2012).
- [20] L. B. Fletcher, H. J. Lee, T. Döppner, E. Galtier, B. Nagler, P. Heimann, C. Fortmann, S. LePape, T. Ma, M. Millot *et al.*, Ultrabright x-ray laser scattering for dynamic warm dense matter physics, *Nat. Photonics* **9**, 274 (2015).
- [21] O. Ciricosta, S. M. Vinko, B. Barbrel, D. S. Rackstraw, T. R. Preston, T. Burian, J. Chalupský, B. I. Cho, H.-K. Chung, G. L. Dakovski *et al.*, Measurements of continuum lowering in solid-density plasmas created from elements and compounds, *Nat. Commun.* **7**, 1 (2016).
- [22] C. Pellegrini, A. Marinelli, and S. Reiche, The physics of x-ray free-electron lasers, *Rev. Mod. Phys.* **88**, 015006 (2016).
- [23] A. A. Lutman, J. P. MacArthur, M. Ilchen, A. O. Lindahl, J. Buck, R. N. Coffee, G. L. Dakovski, L. Dammann, Y. Ding, H. A. Dürr *et al.*, Polarization control in an x-ray free-electron laser, *Nat. Photonics* **10**, 468 (2016).
- [24] J. M. J. Madey, Stimulated emission of bremsstrahlung in a periodic magnetic field, *J. Appl. Phys.* **42**, 1906 (1971).
- [25] A. B. Temnykh, Delta undulator for Cornell energy recovery linac, *Phys. Rev. ST Accel. Beams* **11**, 120702 (2008).
- [26] Z. Huang and K. J. Kim, Review of x-ray free-electron laser theory, *Phys. Rev. ST Accel. Beams* **10**, 034801 (2007).

- [27] See Supplemental Material at <http://link.aps.org/supplemental/10.1103/PhysRevLett.131.073601> for additional details of theory, which includes Refs. [28–32].
- [28] H. Mitter, Quantum electrodynamics in laser fields, in *Electromagnetic Interactions and Field Theory* (Springer Verlag, Berlin, 1975), pp. 397–468.
- [29] H. Casimir, Über die intensität der streustrahlung gebundener elektronen, *Helv. Phys. Acta* **6**, 287 (1933).
- [30] L. Mandel and E. Wolf, *Optical Coherence and Quantum Optics* (Cambridge University Press, Cambridge, England, 1995).
- [31] S.A. Hill and W.K. Wootters, Entanglement of a Pair of Quantum Bits, *Phys. Rev. Lett.* **78**, 5022 (1997).
- [32] A. Di Piazza, Completeness and orthonormality of the Volkov states and the Volkov propagator in configuration space, *Phys. Rev. D* **97**, 056028 (2018).
- [33] V. I. Ritus, Quantum effects of the interaction of elementary particles with an intense electromagnetic field, *J. Sov. Laser Res.* **6**, 497 (1985).
- [34] E. Lötstedt and U. D. Jentschura, Nonperturbative Treatment of Double Compton Backscattering in Intense Laser Fields, *Phys. Rev. Lett.* **103**, 110404 (2009).
- [35] E. Lötstedt and U. D. Jentschura, Correlated two-photon emission by transitions of Dirac-Volkov states in intense laser fields: QED predictions, *Phys. Rev. A* **80**, 053419 (2009).
- [36] W. K. Wootters, Entanglement of Formation of an Arbitrary State of Two Qubits, *Phys. Rev. Lett.* **80**, 2245 (1998).